

Response to RC1:

This study developed a method to calibrate key parameters in Demeter, a community spatial downscaling model, by using a long-term global satellite-based land cover dataset. The sensitivities of the key parameters and propagation of the uncertainties in the projection were also evaluated. The parameterization in the Demeter is important for a better performance of downscaling land use and land cover data from projection at the regional level. I'd recommend accepting this paper upon some minor revisions.

- *We thank the reviewer's positive comments on the importance of this paper. Below we respond the reviewer's specific comments point-by-point.*

1. The section of introduction needs to be improved. The first paragraph discussed multiple topics such as background and motivations. They can be separated as individual paragraphs for readers' understanding. The challenges can also be briefly discussed in the introduction.

- *We have separated the second paragraph in the original manuscript into two paragraphs. In the first paragraph of the revised "introduction" section, we introduced the critical role of LULCC in the Earth system science research, followed by the statement of motivation of studying spatial downscaling of LULCC by the integrated Human-Earth system models such as GCAM. In the third paragraph, we added sentences for introducing other spatial disaggregation models as suggested by RC2, and briefly discussed the challenges of determining Demeter parameters. See Line 55-77.*

2. Although the Demeter has been published, an overview illustration of this model will be very helpful for readers to understand the work in this paper without reading the Demeter paper.

- *We added a figure to provide an overview of Demeter's key processes. Please see Figure S1 in the supplementary materials.*

3. As this paper focused on the calibration of parameters, these parameters are important and deserve some explanations. For example, it is not clear what is selection threshold.

- *We added further clarifications to the parameters and associated variables. Please see Line 105-106 and Line 115-116.*

4. I read the paper in pdf. I found the symbols in the equations do not show up. They are "sum"?

- *We have made modifications to the equations to make sure they show up correctly.*

5. Figure 7 can be improved regarding readability. For example, some boundaries of AEZ can be removed?

- *We improved the quality of Figure 7 and the related Figure S2-S6 in the supplementary file by reducing the visibility of the AEZ boundaries.*

6. Figure 8 can be improved.

- *We have improved the quality of Figure 8 and made modifications with the results of using “top 10%” parameters as suggested by reviewer 2.*

7. Figure 8: I expected the uncertainty will increase monotonously. But for some land cover types, it even decreases after the middle of the century. Any explanations?

- *We thank the reviewer identify this problem. We found a mistake in preparing Figure 8. All the uncertainties increase monotonously after the correction.*

8. This study is an important contribution to the development of the community spatial downscaling model, Demeter. It is still worth to discuss the limitations and future directions. For example, a set of global parameters were used in the Demeter. Further efforts should be made for the regional level and even AEZ level parameterization, especially with the capability of parallelized computing. The second effort should be made in the future work is the improvement of urban land use. Currently, the performance of urban land use is not good as other land cover types. It could be due to the limited consideration of complex urbanization process as well as the input historical urban data. More spatially and temporally consistent urban extent data can be explored (references: A global map of urban extent from nightlights; A global record of annual urban dynamics (1992–2013) from nighttime lights) in the future research. With some minor revisions, I would like to see this paper published.

- *We thank the reviewer’s valuable suggestions. We have inserted a paragraph of discussion on the limitations of current version of Demeter and its parameterization, and pointed out future study directions such as regional/AEZ-level parameterization and improving urban parameterization with satellite-derived urban records. Please see Lines 383-401.*

Response to RC2:

General Comments: The paper presented a thorough investigation of the sensitivity of a global land cover / land use downscaling model (Demeter) to its six model parameters. The work provides essential foundation for making better use of Demeter, and is worth publishing. From a user's point of view, I would appreciate the following suggested modifications made, which collectively ask the authors to further interpret their experiment results and form actionable suggestions for Demeter applications.

- *We thank the reviewer's excellent suggestions. We have added further clarifications, suggestions and discussions accordingly, as elaborated below.*

Specific Comments:

1. The authors argued "equifinality" is present with multiparameter models like Demeter, and presented the optimal setting and top 5% performance setting. It would be useful to see the top few (say, 5-10) "equifinality" parameter settings.

- *We have illustrated the top 10% parameters and the resulted uncertainties in future LULCC downscaling in the revised Figure 2, Figure 8 and Figure S8. Overall, the top 10% parameters will result larger uncertainties than the top 5% parameters, but in a similar way. We also added a short discussion on it in the revised text. Please see Lines 252-255 and 321-322.*

2. The manuscript showed attempts to make suggestions for general users of Demeter, but they need to be more specific and explicit to be useful. For example, the ideal weight for soil nutrient is 0 (figure 2), meaning the model is better off without considering this input variable. Then, the implication for Demeter users is that, users don't need to worry if they don't have good input for this variable, and should focus on getting better quality input for variables that the model is more sensitive to.

- *We have made specific suggestions such as "the users should focus more on the quality of other parameters such as r and τ to which the model is more sensitive", and "We also noticed that the optimal weight for soil nutrient availability for calculating the suitability indices is zero (Figure 2) and the model. A possible reason is that the soil nutrient availability has similar spatial distribution as the cropland in ESA-CCI data, thus provides little additional information in constraining the downscaling processes (Figure S10). This result suggests that the users could ignore the input of soil nutrient availability if it is not available or difficult to collect, and the quantification of the downscaling uncertainty is not required". Please see our revised text in Lines 347-348 and 351-356.*

3. Regional applications of Demeter: The authors stated that different regions differ from the global "average" situation in their own ways, and regional applications of Demeter require "careful" tuning, but provided no further suggestions. Although this paper focuses on a global application of Demeter and global applications are different from regional ones, the authors have learned much about the model's sensitivity, and are better positioned than any user out there to infer what are good starting points (e.g. a range of values to try first, proper sizes of increments when changing values of specific variables) when parameterizing Demeter for regional uses.

This doesn't need to be long, but given the authors' knowledge about the topic, even some speculations would be helpful, but they need to be actionable.

- *We extended our discussion on the regional applications. Specifically, we suggest that users review local historical land use changes, and use the global optimal parameters as a starting point for further parameter adjustment in regional applications. See Line 383-387.*

4. Global applications: The authors presented the optimal set of parameters for global applications, then made some vague suggestions for (global) modeling tuning. Since the authors' experiment is global, it seems the optimal parameters have been identified for global applications. In what cases would global tuning be needed? And what are good starting points for such tuning?

- *We extended our discussion on the global applications as revisions in the Section 4. We suggest urban area downscaling will need to be improved in future applications and the calibrated parameters can be used as a good starting point in case further tuning is necessary, e.g., more detailed final land types are needed in the users' applications. See Lines 388-401 and 410-413.*

5. Demeter's residuals show very strong spatial patterns / biases (figure 7). Some explanations about why it occurred and how it may be moderated (if possible) would be useful.

- *We added a few sentences to introduce Demeter and other spatial downscaling models, as well as the differences between Demeter and the other models in introduction. Please see Lines 293-300.*

Technical Corrections:

1. The authors mentioned how Demeter compare to other spatial downscaling models, but it came up in the method section. It would be nice to see that in introduction.

- *We added a few sentences to introduce Demeter and other spatial downscaling models, as well as the differences between Demeter and the other models in introduction. Please see Lines 55-62.*

2. Many equations are not displayed properly in my copy of the manuscript. Equation (5) especially is not readable at all.

- *We have made modifications to the equations to make sure they show up correctly.*

3. Table 1 showing land cover conversion priorities must label whether rows/cols are origin/destination land cover types, because the conversion priorities are not symmetric.

- *We have added 'Origins' and 'Destinations' labels in Table 1 and descriptions in the table caption.*

4. Ln 152: "Y is the model outputs (i.e., E)" and the following equation $E(Y|X)$ are confusing. Usually, $E(Y)$ denotes the statistical expectation of Y.

- *We used θ and ε to replace X and Y in the calculation of Sobol indices to avoid confusion, and clarified Var and E are statistical variance and expectation.*

Response to SC1:

Dear authors, in my role as Executive editor of GMD, I would like to bring to your attention our Editorial version 1.1: <http://www.geosci-model-dev.net/8/3487/2015/gmd-8-3487-2015.html>

This highlights some requirements of papers published in GMD, which is also available on the GMD website in the ‘Manuscript Types’ section: http://www.geoscientific-modeldevelopment.net/submission/manuscript_types.html

In particular, please note that for your paper, the following requirement has not been met in the Discussions paper: "The main paper must give the model name and version number (or other unique identifier) in the title." As I understand from the abstract, the real model development published here is demeter. Therefore please add the models name and version number to the title of your revised manuscript. E.g. "Calibration and analysis of the uncertainty in downscaling global land use and land cover projections from GCAM using DEMETER (v x.y)".

- *We have updated the title as “Calibration and analysis of the uncertainty in downscaling global land use and land cover projections from GCAM using Demeter (v1.0.0)”*

Additionally, please note, that GMD is encouraging authors to provide a persistent access to the exact version of the source code used for the model version presented in the paper. As explained in https://www.geoscientific-modeldevelopment.net/about/manuscript_types.html the preferred reference to this release is through the use of a DOI which then can be cited in the paper. For projects in GitHub (such as demeter) a DOI for a released code version can easily be created using Zenodo, see <https://guides.github.com/activities/citable-code/> for details.

- *We have added the DOI in the revised manuscript. See Line 60.*

1 **Calibration and analysis of the uncertainty in downscaling global land use and**
2 **land cover projections from GCAM using Demeter (v1.0.0)**

3

4 Min Chen^{1*}, Chris R. Vernon², Maoyi Huang², Katherine V. Calvin¹, and Ian P. Kraucunas²

5

6 ¹ Joint Global Change Research Institute, Pacific Northwest National Laboratory, College Park, Maryland
7 20740, United States

8 ² Atmospheric Sciences and Global Change Division, Pacific Northwest National Laboratory, P.O. Box
9 999, Richland, Washington 99352, United States

10

11 *Corresponding author

12 Email: min.chen@pnnl.gov

13 Telephone: 1-301-314-6755

14 Fax: 1-301-314-6719

15 **Abstract**

16 Demeter is a community spatial downscaling model that disaggregates land use and land cover
17 changes projected by integrated human-Earth system models. Demeter has not been intensively
18 calibrated, and we still lack a good knowledge about its sensitivity to key parameters and the parameter
19 uncertainties. We used long-term global satellite-based land cover records to calibrate key Demeter
20 parameters. The results identified the optimal parameter values and showed that the parameterization
21 substantially improved the model's performance. The parameters of intensification ratio and selection
22 threshold were the most sensitive and needed to be carefully tuned, especially for regional applications.
23 Further, small parameter uncertainties after calibration can be inflated when propagated into future
24 scenarios, suggesting that users should consider the parameterization equifinality to better account for the
25 uncertainties in the Demeter downscaled products. Our study provides a key reference for Demeter users,
26 and ultimately contribute to reducing the uncertainties in Earth system model simulations.

27

28 **Key words:** Demeter; land use and land cover change; parameterization; human-Earth systems models

29

30 **1. Introduction**

31 Land Use and Land Cover Change (LULCC) represents one of the most important human impacts on
32 the Earth system (Hibbard et al., 2017). Besides its socioeconomic effects, LULCC is directly linked to
33 many natural land surface processes, such as land surface energy balance, carbon and water cycle (e.g.,
34 Piao *et al* 2007, Law *et al* 2018, Sleeter *et al* 2018, Pongratz *et al* 2006), and indirectly affects the climate
35 system (e.g., Dickinson and Kennedy 1992, Findell *et al* 2017, Costa and Foley 2000). Thus, LULCC has
36 been considered as a key process in simulating of Earth system dynamics, and LULCC inputs at
37 appropriate time steps and spatial resolutions are required to match the setup of the Earth System Models
38 (ESMs) and the nature of spatial heterogeneity of the Earth system processes (Brovkin et al., 2013;
39 Lawrence et al., 2016; Prestele et al., 2017).

40 While recent historical LULCC information can be obtained by ground investigation or satellite
41 remote sensing (Friedl et al., 2002; Hansen et al., 2000; Loveland et al., 2000; Zhang et al., 2003),
42 projections of future LULCC largely rely on mathematical models that bring socioeconomic and other
43 diverse sectoral information together in a coherent framework to simulate the interactions between natural
44 and human systems. However, these integrated models project LULCC at subregional level, i.e., the basic
45 spatial units that have uniform properties for every sector (e.g., agricultural, energy and water etc.),
46 typically ranging from a few hundred to millions of square kilometers (Edmonds et al., 2012). For
47 example, the GCAM model has been widely used to explore future societal and environmental scenarios
48 under different climate mitigation policies which provides LULCC projections at region-agroecological
49 or water basin level (Edmonds et al., 1997; Edmonds and Reilly, 1985; Kim et al., 2006). ESMs divide
50 the Earth surface into a number of grid cells and the forcing data have to be available at the same spatial
51 resolution to drive the ESMs (Taylor et al., 2012). Therefore, spatial downscaling of the subregional
52 LULCC becomes a critical step for linking models like GCAM and ESMs to investigate the effects of the
53 LULCC on the processes in the natural world, and further the interactions between the human and natural
54 systems (Hibbard and Janetos, 2013; Lawrence et al., 2012).

55 There has been a few spatial disaggregation studies for LULCC, e.g., the Global Land Use Model
56 (Hurtt et al., 2011) and a dynamic global land use model (Meiyappan et al., 2014) with various
57 geographical and socioeconomic assumptions. In previous studies, we have developed a new simple and
58 efficient LULCC downscaling model, named Demeter, to bridge GCAM and ESMs (Le Page et al., 2016;
59 Vernon et al., 2018; West et al., 2014), and made it available online at
60 <http://doi.org/10.5281/zenodo.1214342> . Comparing to other models, Demeter makes minimal
61 assumptions of the socioeconomic impacts. Instead, it uses a few parameters to implicitly characterize the
62 spatial patterns of land use changes (See introductions in Section 2.1). Demeter has been successfully
63 applied at both global (Le Page et al., 2016) and regional (West et al., 2014) levels for downscaling
64 GCAM-projected land use and land cover changes, and has been further developed with an extensible

Deleted: land use and land cover change

Deleted: .

67 output module which streamlines producing specific output formats required by various ESMs (Vernon et
68 al., 2018). However, ~~Demeter's parameters (discussed in Section 2.1), which conclude many geographic~~
69 ~~patterns of long-term land cover changes such as intensification and expansion, are difficult to determine~~
70 ~~by either literature review or simple mathematical calculations. Therefore,~~ Demeter's parameter values
71 ~~were~~ empirically determined and a complete analysis on Demeter's parametric sensitivity and
72 uncertainties as well as a rigorous model calibration has not been conducted to help minimize the
73 propagation of downscaling errors. ~~In recent years, a growing number of long-term global remote-~~
74 ~~sensing-based LULCC datasets are made available (e.g., the Land Cover project of the European Space~~
75 ~~Agency Climate Change Initiative, MODIS Land Cover product collections 6), it becomes possible to use~~
76 ~~these datasets to calibrate Demeter parameters. The major objective of this study is to develop a~~
77 framework for calibrating the key parameters of Demeter, testing and quantifying the parameter
78 sensitivities and uncertainties, and demonstrating how the parameter uncertainties would affect
79 downscaled products.

Deleted: There has been a few spatial disaggregation models developed for LULCC, e.g., the Global Land Use Model (Hurtt et al., 2011) and the dynamic global land use model developed (Meiyappan et al., 2014)

Deleted: have been

Deleted: While

Deleted: there are

Deleted: i

Deleted: T

81 2. Method

82 2.1 Demeter

83 Demeter is a land use and land cover change downscaling model, which is designed to disaggregate
84 projections of land allocations generated by GCAM and other models. For example, GCAM projects land
85 cover areas in each of its spatial units (e.g., region-agro-ecological zones, region-AEZ) for each land
86 cover type, and Demeter uses gridded observational land cover data (e.g., satellite-based land cover
87 product) as the reference spatial distribution of land cover types and allocates the GCAM-projected land
88 area changes to grid level at a target spatial resolution, following some user-defined rules and spatial
89 constraints (Figure S1). Below we briefly summarize the key processes of Demeter, and the detailed
90 algorithms can be found in three earlier publications (Le Page et al., 2016; Vernon et al., 2018; West et
91 al., 2014).

92 Demeter first reconciles the land cover classes defined in the parent model and the reference dataset
93 to user-defined unified final land types (FLTs). Downscaled land cover types will be presented in FLTs.
94 For example, if Demeter reclassifies the 22 GCAM land cover types and the 16 International Geosphere-
95 Biosphere Programme (IGBP) land cover types from the reference dataset into 7 FLTs (Forest, Shrub,
96 Grass, Crops, Urban and Sparse), the 7 FLTs will be the land types represented in Demeter's outputs by
97 default. Demeter then harmonizes the GCAM-projected land cover areas and the reference dataset at the
98 first time step (or 'base year') to make sure they are consistent with the GCAM spatial units and allocates
99 the projected land cover changes by intensification and extensification. Intensification is the process of
100 increasing a particular land cover in a grid cell where it already exists, while extensification creates new
101 land cover in grid cells where it does not yet exist but is in proximity to an existing allocation. The order

111 of transitions among land cover types is defined by “transition priorities” during the processes of
 112 intensification and extensification. A parameter (r , from 0 to 1) is defined as the ratio of intensification,
 113 and thus $1-r$ of the land cover change is for extensification. Proximal relationships are defined by spatial
 114 constraints that determine the probability that a grid cell may contain a particular land use or land cover
 115 class. The current Demeter setup includes three spatial constraints: kernel density (KD), soil workability
 116 (SW) and nutrient availability (NA). KD measures the probability density of a land cover type around a
 117 given grid cell, and SW and NA are normalized scalars (0~1) for agricultural suitability. For each land
 118 cover type and grid cell, KD is calculated by the spatial distance (D) at the runtime, and SW and NA are
 119 estimated from the Harmonized World Soil Database (HWSD, FAO/IIASA/ISRIC/ISSCAS/JRC, 2012).
 120 A suitability index (SI) from 0 to 1 is defined as the weighted-average of the three spatial constraints to
 121 assess how suitable a grid cell is to receive a land cover type:

122
$$SI = (w_K * KD + w_S * SW + w_N * NA) / (w_K + w_S + w_N) \quad (1)$$

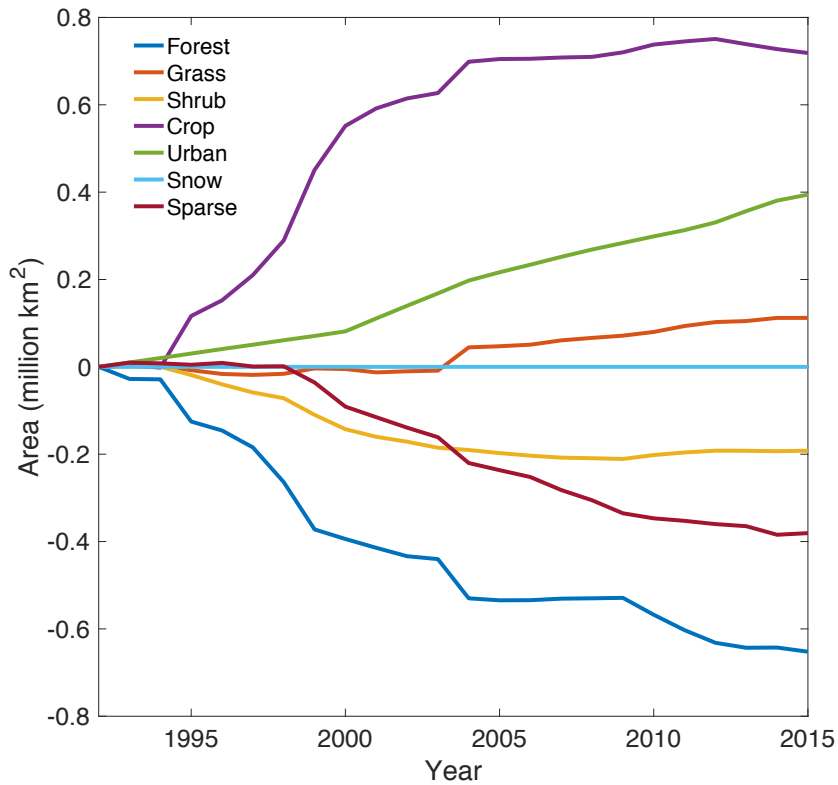
123 where w_K , w_S , and w_N are the weights for KD, SW and NA, respectively, and the sum of them is 1. In the
 124 process of extensification, Demeter ranks candidate grid cells based on their suitability indices and selects
 125 the most suitable candidate grid cells following a user-defined threshold percentage (τ) for extensification.
 126 In other words, τ determines the number of grid cells to be selected and used for the tentative and actual
 127 conversion of land cover types.

128
 129 Table 1. Transition priorities by analyzing the 24-year global land cover records from the Land Cover
 130 CCI project of the European Space Agency Climate Change Initiative. The rows and columns represent
 131 the origins and destinations of the transitions, respectively. The smaller numbers indicate higher transition
 132 priorities.

Final Land Types (origins)	Final Land Types (destinations)						
	Forest	Shrub	Grass	Crop	Urban	Snow	Sparse
Forest	0	2	3	1	4	5	6
Shrub	2	0	3	1	4	5	6
Grass	1	2	0	3	5	6	4
Crop	2	3	1	0	5	6	4
Urban	1	4	3	2	0	6	5
Snow	2	3	4	1	5	0	6
Sparse	2	3	4	1	5	6	0

133
 134 2.2 Calibrate Demeter with historical land cover record and sensitivity analysis

139 As indicated above, users should define a few parameters including the treatment order, the transition
140 priorities for allocating the land cover changes, the intensification ratio r , the selection threshold τ , the
141 radius for calculating kernel density D , and weights for the spatial constraints (w_K , w_S , and w_N), in order to
142 use Demeter for downscaling projected land cover change. These parameters were determined empirically
143 in previous studies. Here we calibrated these parameters for Demeter using a time series of global land
144 cover records from the Land Cover project of the European Space Agency Climate Change Initiative
145 (referred to as CCI-LC products hereafter). The CCI-LC products have been generated by critically
146 revisiting all algorithms required for the generation of a global land cover product from various Earth
147 Observation (EO) instruments, thus provide a globally consistent land cover record over two decades
148 (1992-2015). The CCI-LC products are available at 300 m spatial-resolution and annual time step and
149 classify the global land cover into 38 groups. We reclassified the CCI-LC products into the default 7
150 FLTs (Table S1) and resampled them into 0.25° resolution with the official software tools, following the
151 description of CCI-LC products in the user guide
152 (http://maps.elie.ucl.ac.be/CCI/viewer/download/ESACCI-LC-Ph2-PUGv2_2.0.pdf). Figure 1 shows
153 large interannual global changes for the 7 FLT areas, especially for the forests and croplands, which have
154 decreased and increased over 0.6 million km² over the past two decades, respectively. We used the
155 gridded 0.25° CCI-LC over the 24-year period as the observational data (below referred to “LC-grid-
156 obs”) and aggregated them into GCAM’s region-AEZ level to produce a synthetic GCAM-projected land
157 cover change (below referred to “LC-AEZ-syn”). In this way, we can apply Demeter to LC-AEZ-syn to
158 calibrate Demeter with the LC-grid-obs by tuning the parameters of Demeter.
159



160
 161 Figure 1. Interannual changes of global Final Land Types (FLT) areas over 1992-2015 relative
 162 to 1992, as indicated by the ESA CCI-LC product.

163 A preliminary sensitivity analysis of Demeter indicated that the downscaled results are not sensitive
 164 to treatment order and transition priorities (Le Page et al., 2016), thus we used the default treatment order,
 165 i.e., from least to greatest: Urban, Snow, Sparse, Crops, Forest, Grass, Shrub. We decided the transition
 166 priorities by sorting the probabilities of transitioning one FLT to another based on the 24-year CCI-LC
 167 record (Table 1). To calibrate the other six parameters (r , τ , w_K , w_S , w_N and D), we sampled their values at
 168 equal intervals (Table 2) and generated all possible combination (23,100 in total) for a Monte-Carlo
 169 ensemble Demeter downscaling experiment, using LC-AEZ-syn as the input. The Monte-Carlo
 170 experiment generated 23,100 sets of downscaled 0.25-degree global land use and land cover areas, which

171 were compared against LC-grid-obs to calculate their similarities to the observational data, ranked by
 172 their discrepancies from the least to greatest to determine the likelihood of the parameters. We calculated
 173 the discrepancies as the root mean square error (E_y) between the downscaled and observed land cover
 174 areas for each year:

$$E_y = \sqrt{\frac{1}{G} \frac{1}{L} \sum_g^G \sum_l^L (Ad_{y,l,g} - Ad_{o,l,g})^2} \quad (2)$$

175 and the average of the discrepancies over the years (E):

$$E = \frac{1}{Y} \sum_y^Y E_y \quad (3)$$

176 where g is the index for G grid cells over the globe ($G = 265,852$), l is the index for the L FLTs ($L = 8$), y
 177 is the index for Y years. We chose 1992, 2000, 2005, 2010 and 2015 to keep consistent with the GCAM
 178 time steps, thus $Y = 5$. $Ad_{y,l,g}$ and $Ad_{o,l,g}$ are the downscaled and observational land cover areas for grid
 179 cell g , FLT l and year y . The unit for E_y and E is km^2 .

182 To test the model sensitivity to these key parameters, we conducted a sensitivity analysis using the
 183 results from the Monte-Carlo experiment. The first-order and total-order Sobol sensitivity indices were
 184 used to identify the model sensitivity to each of the six parameters (Saltelli et al., 2004). Let θ_i denotes the
 185 i th parameter ($i=1, \dots, n$, here $n=6$), ε_y is the model outputs (i.e., the discrepancies between downscaled and
 186 observed land cover areas), the first-order Sobol index (S_i) is defined as:

$$S_i = \frac{\text{Var}[E(\varepsilon | \theta_i)]}{\text{Var}(\varepsilon)} \quad (4)$$

187 Here Var and E are the statistical variance and expectation. And the total-order Sobol index (S_{Ti}) is
 188 defined as the sum of sensitivity indices at any order involving parameter θ_i , where $S_{ijk \dots n}$ denotes the n th-
 189 order sensitivity index:

$$S_{Ti} = S_i + \sum_{j=1, j \neq i}^n S_{ij} + \sum_{j,k=1, j,k \neq i}^n S_{ijk} + \dots + \sum_{j,k \dots n=1, j,k \dots n \neq i}^n S_{ijk \dots n} \quad (5)$$

191 The first-order Sobol index represents the contribution to the output variance of the main effect of θ_i ,
 192 therefore it measures the effect of varying θ_i alone; and the total-order Sobol index measures the
 193 contribution to output variance of θ_i and includes all variance caused by its interactions with other
 194 parameters. Larger Sobol indices indicate higher parameter sensitivities.

Deleted: X

Deleted: Y

Deleted: E

$$S_i = \frac{\text{Var}[E(Y | X_i)]}{\text{Var}(Y)}$$

Deleted: X

Formatted: Font: Italic

Formatted: Font: Italic

Deleted: X

Deleted: X

Deleted: X

Deleted: X

207 Table 2. Key parameters, and their sampling range and steps for calibration in this study.

Name	Definition	Min	Max	Sampling step
w_N	Weight of soil nutrient availability for calculating suitability index	0	1	0.2
w_S	Weight of soil workability for calculating suitability index	0	1	0.2
w_K	Weight of kernel density for calculating suitability index	0	1	0.2
r	Intensification ratio	0	1	0.1
τ	Selection threshold	0	1	0.1
D	Kernel radius	10	100	10

208

209 *2.3 Propagate the parameter uncertainties to GCAM LULCC downscaling*

210 We selected parameter combinations which produced the smallest 5% E_s based on their rankings
 211 from the Monte-Carlo experiment, and used them as ‘acceptable’ parameters to represent the parameter
 212 uncertainties after calibration. We used Demeter with these parameters to downscale the GCAM-
 213 projected LULCC at 5-year time step from 2005 to 2100 under a reference scenario to examine the
 214 uncertainties of land cover areas for each FLT to demonstrate how different the downscaled LULCC can
 215 be induced by the uncertain parameters. The reference scenario is a business-as-usual case with no
 216 explicit climate mitigation efforts that reaches a higher radiative forcing level of over 7 W m^{-2} in 2100.
 217 We only saved the downscaling results in 2005, 2010, 2050 and 2100 considering the size of the output
 218 files and computational cost. Finally, we calculated the standard deviation across the downscaled land
 219 cover areas for each FLT driven by different parameter combinations, which indicates the parameter-
 220 induced model uncertainties.

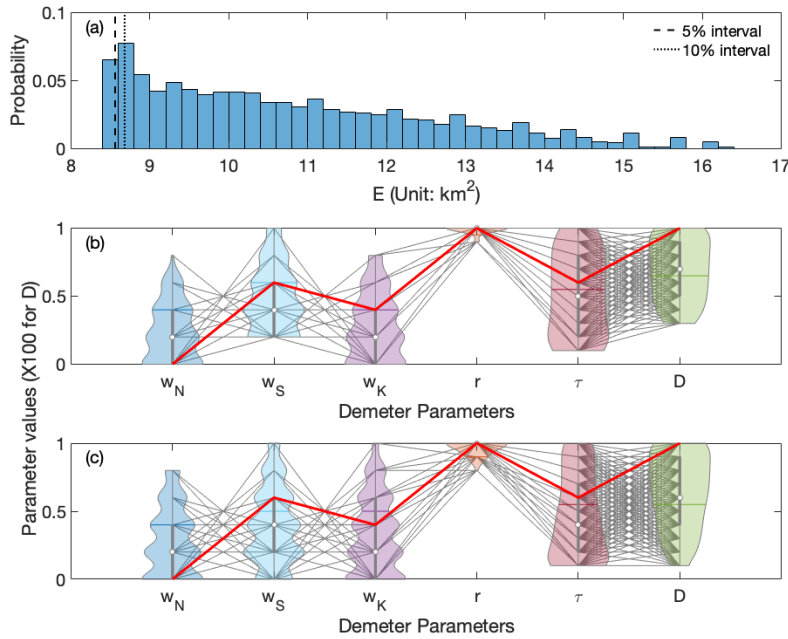
221

222 **3. Results**

223 *3.1 Parameter estimation and sensitivity*

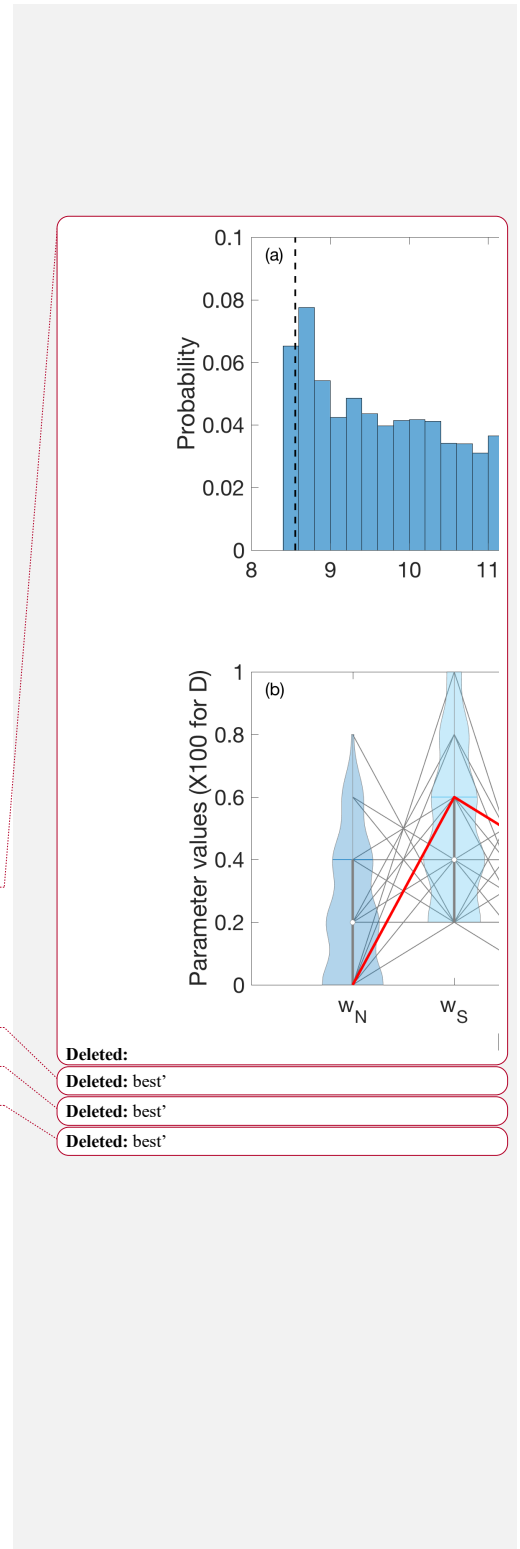
224 The Monte-Carlo Demeter experiment driven by the 23,100 ensemble parameter sets produced
 225 diverse downscaled LULCC realizations. As shown in Figure 2a, the disagreements between the
 226 downscaled FLT fraction and the reference record, measured by the average root mean square error (E_s ,

227 Equation 3) for all the FLTs and grid cells over the five years (1992, 2000, 2005, 2010 and 2015), are
 228 mainly distributed between 8 and 17 km² (about 1%-3% of the area of a 0.25-degree grid cell).

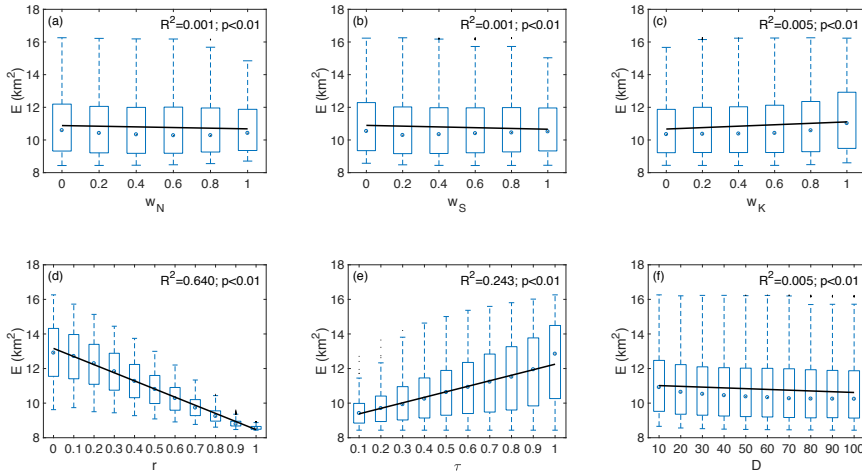


229
 230 Figure 2. (a) Histogram of the E_s , i.e., the global average discrepancies between the downscaled
 231 and observed land cover areas with the 23,100 ensemble parameter sets; the vertical dashed line
 232 in (a) shows the interval of the ‘acceptable’ 5% parameters, as described in Section 2.3; (b) the
 233 probability density of each of the ‘acceptable’ 5% parameters, as shown by the violin plots; the
 234 black lines across the six parameters show all the ‘acceptable’ 5% parameter sets, and the red
 235 line indicates the global optimal parameter values; the box plots and horizontal bar inside the
 236 violin plots indicate the interquartile ranges and the mean of the parameter values, respectively.
 237 (c) same as (b) but shows the ‘best’ 10% parameter sets. Note that the values of D were divided
 238 by 100 for the purpose of illustration in (b) and (c).

239 Figure 3 shows the relationship between the values of the six parameters and their corresponding E_s ,
 240 resulted from the Monte-Carlo experiment. We found that the E_s are significantly correlated to all the six
 241 parameters ($p < 0.01$). The intensification ratio (r) has the strongest linear correlation with the E_s

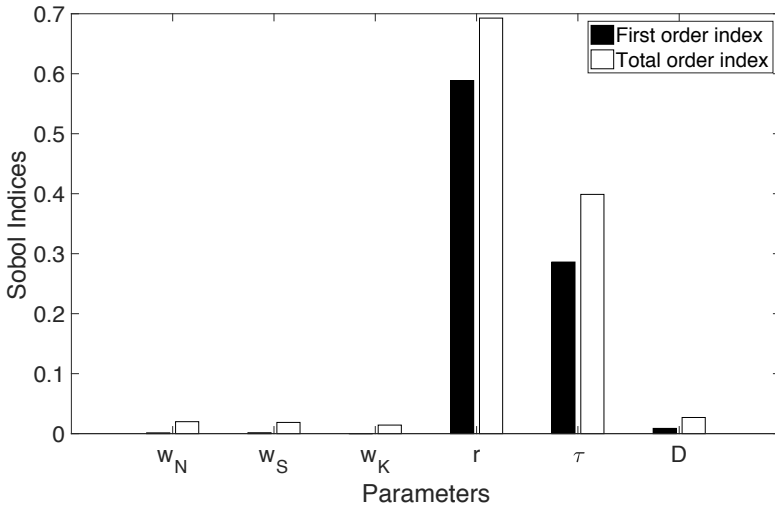


246 ($R^2=0.64$), followed by the selection threshold (τ) ($R^2 = 0.24$). Overall, the parameters w_K and τ are
 247 positively correlated with E_s (positive slopes of the trendlines), while w_N , w_S , r and D hold negative
 248 correlations, indicating that smaller w_K and τ , and larger w_N , w_S , r and D are associated with smaller E_s .



249
 250 Figure 3. Relationships between the six Demeter parameters and the global average
 251 discrepancies between the downscaled and observed land cover areas (E_s) resulted from the
 252 Monte-Carlo ensemble experiment. Box plots shows distributions of the E_s and the solid lines
 253 show the linear trends.

254 Figure 4 shows the first-order and total-order Sobol indices calculated with the parameter ensemble
 255 and the associated E_s . As indicated by the first-order Sobol indices, the intensification ratio r directly
 256 contributes about 59% to the variability of the E_s , followed by the selection threshold τ and kernel radius
 257 D , which directly contribute 29% and 1% to the variability of the E_s . The other parameters (w_N , w_S and
 258 w_K) have little direct contributions to the E variability. The total-order Sobol indices showed similar order
 259 of parameter importance. r and its interactions with other parameters contributed about 70% of the E
 260 variability, τ contributed about 40%, D contributed about 3%, and w_N , w_S and w_K contributed 2%
 261 respectively. It is clear that the downscaling error is most sensitive to the intensification ratio, followed by
 262 the selection threshold, but not sensitive to the kernel radius and the weighting factors of the spatial
 263 constraints.



264

265 Figure 4. Sobol sensitivity indices for the six Demeter parameters. Higher indices indicate higher
 266 sensitivities.

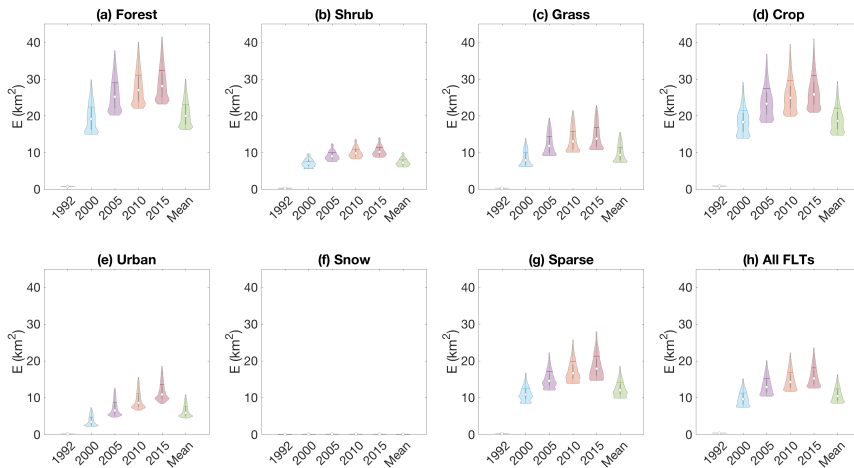
267 We identified the ‘best’ parameters, which are associated with the lowest E , and marked them as the
 268 red line in Figure 2b. We also selected ‘acceptable’ parameters that have E_s lower than 5% quantile in
 269 Figure 2a (hereafter referred to as ‘top 5% parameters’) and thus have the similar performance as the
 270 ‘best’ parameters (differences of $E < 1\%$), and used them to represent the uncertainty of the parameters
 271 shown as the probability density distributions in Figure 2b. The best w_N , w_S , w_K , r , τ and D are 0, 0.6, 0.4,
 272 1, 0.6 and 100, respectively. All the parameters are constrained with the calibration comparing to their
 273 uniform prior distributions. The intensification ratio r has been constrained into a small range (0.9-1.0 and
 274 mostly 1.0) from 0-1.0. Constraining on the other parameters are relatively weaker: w_N , w_S , and w_K have
 275 been narrowed to the ranges of 0-0.8, 0.2-1.0, and 0-0.8, and primarily distributed in 0-0.4, 0.2-0.6 and 0-
 276 0.4 (the first and third quantiles), respectively; τ and D have been constrained into the range of 0.2-1.0
 277 and 30-100 with the first and third quantiles being 0.2-0.8 and 40-90, respectively. This analysis again
 278 indicates that r is the most sensitive parameter, therefore its posterior distribution can be significantly
 279 narrowed through the calibration. In addition, we also selected the ‘acceptable’ parameters that have E_s
 280 lower than 10% quantile (top 10% parameters), as shown in Figure 2a and 2c. Similar distribution of top
 281 10% parameters are found as that of the top 5% parameters, with some small extension on the ranges of
 282 5% parameters.

283

Deleted:

285 3.2 Performance of Demeter in downscaling LULCC

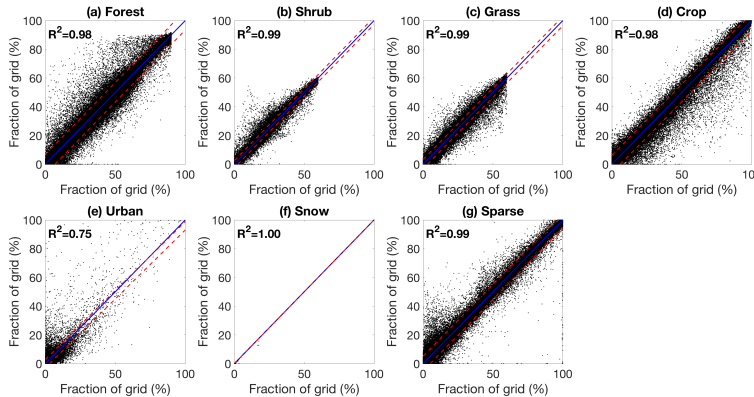
286 Demeter generally performs well in downscaling the synthetic land use and land cover change with
 287 small disagreements with the reference data. For all FLT_s, the disagreements between the downscaled
 288 FLT fraction and the reference record in 1992 (i.e., E_{1992} in Equation 2), are close to zero since we used it
 289 as the harmonization year. The disagreements in 2000 (E_{2000}) are mainly distributed in a range between 5
 290 and 15 km² (about 1%-2% of a 0.25-degree grid cell), with the median about 10 km² and the mean
 291 slightly above 12 km² (Figure 5h). The disagreements increase over years at a rate of about 1 km² per 5-
 292 year time step and reach 13-24 km² (median: 15 km²; mean: 18 km²) in 2015. Overall, the average
 293 disagreements over the five years (E) mainly distributed in 8-17 km² (also shown in Figure 2a), with the
 294 median of about 10 km² and the mean of about 12 km².



295
 296 Figure 5. Possibility densities for the E_s between downscaled and observational Final Land Type
 297 areas for 1992, 2000, 2005, 2010, 2015 and the mean of the five time-steps. The box plots and
 298 horizontal bar inside the violin plots indicate the interquartile ranges and the mean of the
 299 parameter values, respectively. Note that the E_s for Snow are close to 0 thus not visible in the
 300 figure.

301
 302 The errors for each of the FLT_s follow the same increasing trend over the years. Forest and crop have
 303 the largest disagreements between the downscaled and reference distributions with the errors are
 304 primarily located in the range of 20-40 km² in average over the five time steps (Figure 5a,d). The errors
 305 for sparse lands are relatively smaller, which mainly fall into the range of 10-20 km² (Figure 5g),

306 followed by grass, shrub and urban, with the errors are mainly distributed in 0-10 km² averagely over the
 307 five years. Errors for snow is near zero since there was little areal change for this FLT in the CCI-LC
 308 record (Figure 1) and little LULCC allocation was needed in the downscaling process over the years.



309

310 Figure 6. Comparison between the observed and downscaled Final Land Type with optimal
 311 parameters over the 265,852 0.25-degree grid cells in 2015. The blue solid lines show the 1:1
 312 line, and the red dashed lines show the 95% confidence intervals.

313 Figure 6 shows the comparison between reference gridded CCI-LC FLTs and the downscaled FLTs
 314 driven by the best parameters (see Section 3.1) among the 265,852 0.25-degree grid cells in 2015. Except
 315 for urban, the downscaled land cover of other FLTs match the reference record very well (all R² are above
 316 0.98). The R² is 1 for snow due to little change of snow and ice area in the CCI-LC record. Figure 7
 317 demonstrates the spatial distribution of FLT fraction from the reference data and best downscaled results,
 318 together with their differences, using crop as an example. We find that the downscaled results have
 319 successfully reproduced the spatial pattern of crops from the reference data, and similar conclusions can
 320 be drawn for other FLTs (see Figure S2-S6; figure for Snow was not shown because of little change for
 321 this FLT). However, misallocation of the land cover change takes places in most region-AEZs, especially
 322 where LULCC were significant (e.g., Brazil, Eastern China, temperate Africa and Northern Euroasia;
 323 Figure 7 and S1-S5) over the study years, likely due to the application of improper global ratio of
 324 intensification. For example, the Northern China plain has experienced extensive urbanization by
 325 converting a large area of cropland into urbans during the past few decades (Liu et al., 2010). However,
 326 since the calibrated intensification ratio is high (Figure 2), Demeter tends to underestimate the urban
 327 expansion and thus overestimate cropland area at where should be urbanized. Similarly, cropland has
 328 been largely expanded and thus applying a high intensification ratio could not capture such changes.

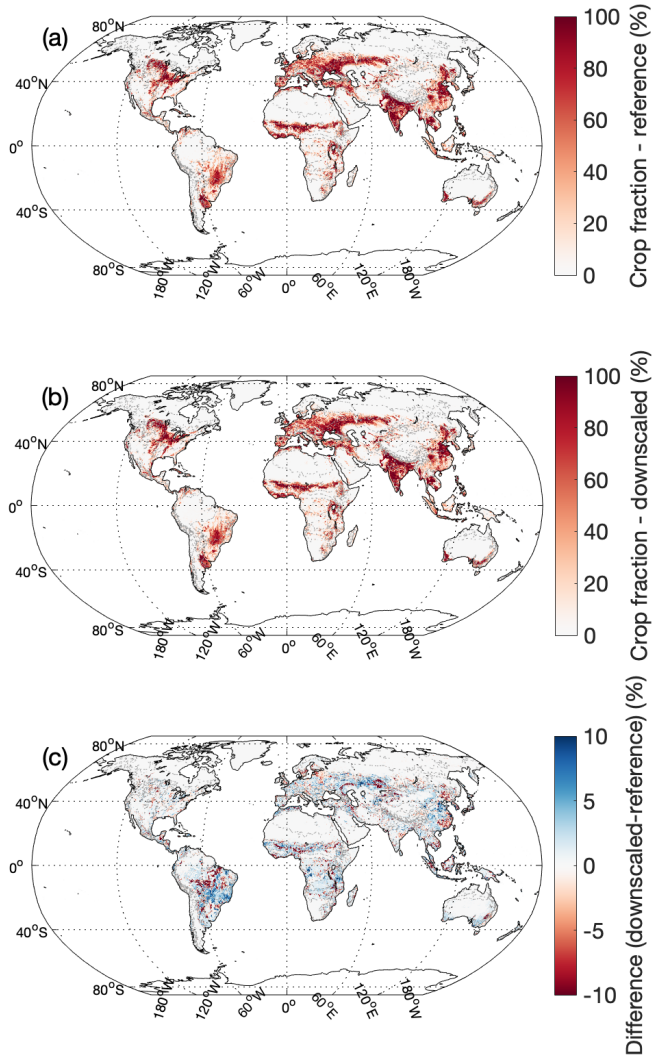
Formatted: Font: 12 pt

Deleted: 1

Deleted: 5

Deleted: Misallocation of the changes primarily takes place in Brazil, China, temperate Africa and Northern Euroasia, where most of the LULCC happened over the study years.

334



335

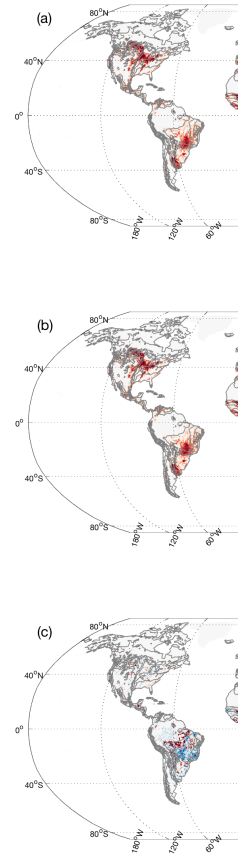
336 Figure 7. Spatial pattern of the observed and downscaled Crop density (measured by percentage
 337 fraction of the grid cell), and their differences in 2015. The grey dot-lines show the boundaries of
 338 the GCAM region-AEZs.

Deleted: ¶

Formatted: Font: 11 pt, Font color: Black

Formatted: Normal, Indent: First line: 0"

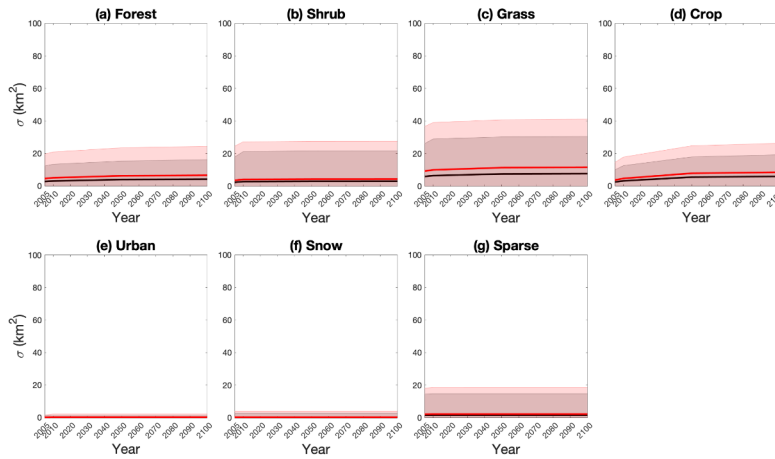
Formatted: Font: 11 pt, Font color: Black



Deleted:

345 3.3 Uncertainty propagation

346 While applying the ‘acceptable’ parameters (top 5% and 10%) in downscaling GCAM projections of
 347 LULCC under the reference scenario, we found that these well-constrained parameters induced
 348 considerable uncertainties in the downscaled results. For each grid cell, we calculated the standard
 349 deviation (σ) of the downscaled land cover areas with different parameters for each FLT. Figure 8 shows
 350 the mean σ of the 265,852 0.25-degree grid cells over the globe for 2005, 2010, 2050 and 2100, as well as
 351 the spatial variability of σ (calculated as the standard deviation over the grid cells and shown as the
 352 shaded area in Figure 8). As shown by the grey lines and shades in Figure 8, the uncertainty of top 5%
 353 parameters has minor effect on downscaled Urban and Snow areas, since GCAM projected little areal
 354 changes of urban and snow. Downscaled sparse areas were slightly affected by the choice of parameters,
 355 indicated by small mean σ (about 2 km² per grid cell). However, the other FLTs, including Forest, Shrub,
 356 Grass and Crop have larger σ s, which also showed an increasing trend over time. The global mean σ for
 357 Forest and Shrub reached about 3 to 4 km² per grid cell and about 6 to 8 km² for Grass and Crop in 2100.
 358 The spatial variability of σ was also larger for these FLTs, for example, the standard deviation of σ
 359 reached over 15 km² per grid cell in 2100 for Crop, and the maximum σ can be over 350 km² per grid cell
 360 in some grid cells (Figure S7). Similar results can be found by using the top 10% parameters, but with
 361 slightly higher magnitudes (red lines and shaded areas in Figure 8 and Figure S8).



362 Figure 8. The Mean (shown as the solid lines) and standard deviations (σ , shown as the shaded
 363 area) for the downscaled Final Land Type (FLT) areas, when propagating the parameter
 364 uncertainties into the GCAM-projected land use and land cover change downscaling in the 21st
 365 century. The black and red colors represent using the top 5% and 10% parameters, respectively.
 366

Deleted: (Figure S6)

Deleted: T

Deleted: little

Deleted: ,

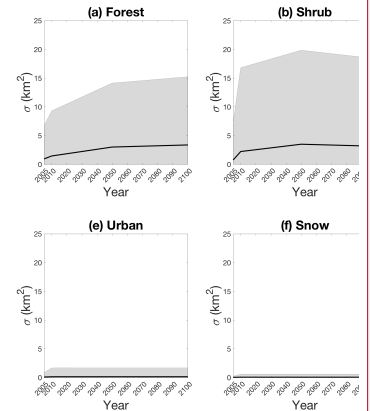
Deleted: and Grass

Deleted: 7.5

Deleted: 6

Formatted: Indent: First line: 0.25", Space After: 0 pt

Deleted: ¶



376 **4. Discussion**

377 To date, there has been only a handful of methods for downscaling projected global land use and land
378 cover change. For example, Oskins *et al* (2016) fitted a statistical model relating coarse-scaled spatial
379 patterns in land cover classes to finer-scaled land cover and other explaining variables. Many more
380 studies used complex land use modeling approach (e.g., Houet *et al* 2017, Oskins *et al* 2016, Meiyappan
381 *et al* 2014, Hurtt *et al* 2011, Souty *et al* 2012) that combines a variety of socioeconomic processes to
382 provide global scale land use allocations. Our results demonstrated that Demeter is an effective tool for
383 downscaling global land use and land cover change, although it adapts a relatively simpler approach.
384 However, choices of parameter values are critically important for a simple model, since it is possible that
385 some complicated processes are simplified to be represented by a single parameter. Although an
386 uncalibrated Demeter can lead to noticeable errors and uncertainties in downscaled land cover areas, our
387 results have shown the effectiveness of the calibration efforts in minimizing the downscaling errors and
388 constraining the uncertainties.

389 A central purpose of our study is to making suggestions for setting up parameters for Demeter's
390 global applications, shown as the global optimal values in Figure 2. Interestingly, we found that the
391 parameters of intensification ratio (ρ) and selection threshold (τ) strongly affected the downscaled results,
392 while the weights of the spatial constraints and kernel radius showed small impacts on the results. This
393 result indicates that the selected spatial constraints (soil workability and nutrient availability) and spatial
394 autocorrelation (measured by kernel density) provide loose constrains on the land allocation in the
395 downscaling process, therefore the users should focus more on the quality of other parameters such as ρ
396 and τ to which the model is more sensitive. In addition, the intensification ratio has been strictly
397 constrained to a range close to 1.0, suggesting that the intensification of land cover, especially cropland,
398 may be the major contributor to the global land use and land cover change, thus spatial constraints on
399 extensification are not very effective. We also noticed that the optimal weight for soil nutrient availability
400 for calculating the suitability indices is zero (Figure 2) and the model. A possible reason is that the soil
401 nutrient availability has similar spatial distribution as the cropland in ESA-CCI data, thus provides little
402 additional information in constraining the downscaling processes (Figure S10). This result suggests that
403 the users could ignore the input of soil nutrient availability if it is not available or difficult to collect, and
404 the quantification of the downscaling uncertainty is not required.

405 There has been a number of numerical methods for model calibration, such as gradient methods
406 (Ypma, 1995), evolutionary algorithms (Ashlock, 2006), and data assimilation techniques (Kalnay, 2002).
407 Our calibration method is relatively simpler, and the sampling steps are relatively coarse. As a result, it is
408 possible that the calibrated parameters can be further improved with a more rigorous calibration strategy,
409 although these biases should be small since the sampling bins are narrow and the sensitive parameters are
410 well constrained (Figure 2). However, our method has a few advantages for this particular global land use

Deleted: as

Formatted: Font: Italic

Formatted: Font: Italic

Deleted: . We also noticed that

413 and land cover change downscaling model calibration problem. First, we sampled the whole parameter
414 space thus our Monte-Carlo downscaling experiments can well represent the parameter uncertainties.
415 Second, the other methods mentioned above typically adjust model parameters and run the model
416 iteratively to find the parameters to hit the local or global minimum cost function value (Chong and Zak,
417 2013), and thus can be very time consuming due to the size of the datasets and the difficulty of algorithm
418 parallelization. The Monte-Carlo ensemble runs of Demeter in our method can be easily parallelized and
419 thus is computationally efficient. Finally, the saved downscaled results from the global Monte-Carlo
420 downscaling experiment can be reused for regional applications. Our study provided an optimal set of
421 Demeter parameters. It is worth noting that these parameters are optimized to minimize the average
422 discrepancies between the downscaled and historically observed land cover areas at the global scale, thus
423 they may need to be recalibrated when Demeter is applied to a particular region. For example, the best
424 estimate of the intensification ratio is 1 for a global downscaling experiment, probably due to that
425 intensification is a more common phenomena than extensification during the past land use and land cover
426 change in the past two decades as recorded by the ESA-CCI data. However, this high intensification ratio
427 for Crop may be more realistic for the regions with long-term agricultural history (e.g., India), while it
428 should become lower for the United States (US) where cropland extensification rapidly happened in the
429 past century. We extracted the grid cells in the conterminous US (grid cells between 25° N and 50° N, and
430 125° W and 65° W) and India (grid cells between 7° N and 33° N, and 68° E and 98° E), and used them
431 together with the same method as the global calibration to determine the optimal parameters for the US
432 and India, which clearly showed that the intensification ratio remained 1 for India, but moved towards
433 lower values for the US (Figure S9). Therefore, we recommend future efforts on examining regional
434 parameterization should be made for Demeter's applications at specific regional/AEZ levels. Since some
435 of the key parameters have clear physical definition (e.g., the intensification ratio), while the global
436 optimal values could be used as a starting point, it would be helpful to review the local historical land use
437 change to infer these parameters when applying Demeter to a specific region.

438 In addition, although the downscaled urban land use can capture most of the variability in reality, it is
439 clear that Demeter's performance for urban is not as good as that for other land cover types (Figure 6). On
440 the other hand, accurate projection of the spatial extent and pattern of urbanization is getting more
441 important for better understanding its environmental, ecological and socioeconomic impacts in such an
442 era of rapid urbanization (Georgescu et al., 2012; Jones et al., 1990; Merckx et al., 2018; Zhang et al.,
443 2018). Thus, a key future effort should be made for improving the downscaling accuracy of urban land
444 use. The relative larger errors could be either due to the limited consideration of complex urbanization
445 processes and the lack of specific parameterization of the urban land cover type. While incorporating
446 better representation of urbanization in Demeter can be more complicated, it is possible to improve the
447 model performance by further parameterizing the model with more historical urban data. For example,

Deleted: 7

Commented [HM1]: Is this partially because that GCAM does not consider urban expansion. Shall we discuss that as well?

449 [global satellite-observed nightlights have been used for mapping urban area](#) (Elvidge et al., 2009; Li and
450 Zhou, 2017b; Zhou et al., 2014) [and producing a global record of annual urban dynamics \(1992-2013\)](#) (Li
451 and Zhou, 2017a), [which will be particularly useful for the future calibration of Demeter on urban](#)
452 [dynamics](#).

453 Model calibration usually can provide several sets of parameters to allow the calibrated model to give
454 similar results, which is called equifinality (Beven and Freer, 2001). As a result, the calibrated parameters
455 become another source of uncertainty in model-simulated results. The equifinality also exists in our
456 calibrations. We have observed noticeable growing uncertainties in downscaled land cover areas while
457 propagating the parameter uncertainties into the Demeter downscaling practices with GCAM projected
458 LULCC in the 21st century. Therefore, while calibration can remarkably reduce the uncertainty of the
459 parameters, it may be better to use sets of constrained parameters rather than a single set of ‘best’
460 parameters in the practice of Demeter, for the purpose of accounting for the parameter uncertainty and
461 providing more reliable land use and land cover change downscaling. [Moreover, it is worth noting that the](#)
462 [calibrated parameters are tuned for FLTs, which we believe have covered most land cover types and are](#)
463 [directly useful in most cases. When the users need to consider more FLTs in their global applications, the](#)
464 [optimal values introduced in this study can be used as a starting point for further tuning](#).

465

466 **5. Conclusions**

467 We developed a Monte-Carlo ensemble experiment for Demeter, a land use and land cover change
468 downscaling model of GCAM, analyzed the model’s sensitivity to its key parameters, and calibrated the
469 parameters to minimize the mismatch between the model-downscaled and satellite-observed land use and
470 land cover change in the past two decades. We identified the optimal parameter values for global
471 applications of Demeter, and showed that the parameterization of Demeter substantially improved the
472 model’s performance in downscaling global land use and land cover change. The intensification ratio and
473 selection threshold turned out to be the most sensitive parameters, thus need to be carefully tuned,
474 especially when Demeter is used for regional applications. Further, the small uncertainty of parameters
475 after calibration can result in considerably larger uncertainties in the results when propagating them into
476 the practice of downscaling GCAM projections, suggesting that Demeter users consider the
477 parameterization equifinality to better account the uncertainties in the Demeter downscaled land use and
478 land cover changes.

479

480

481 **Code Availability**

482 The source code of GCAM and Demeter is available at <https://github.com/JGCRI/gcam-core>

483 and <https://github.com/IMMM-SFA/demeter>. The scripts for performing the calibration and analysis are
484 available at https://drive.google.com/open?id=1qNzh4eKgVcO_BjG2RjAw33whqxSMH8wm.

485

486 **Data Availability**

487 The ESA-CCI data was downloaded from <https://www.esa-landcover-cci.org/>. Other data are available at
488 https://drive.google.com/open?id=1qNzh4eKgVcO_BjG2RjAw33whqxSMH8wm.

489

490 **Author contribution**

491 M.C. conceived the study and all the authors contributed to design the study. M.C. lead the data
492 acquisition and performed the experiment and analysis with technical assistance from C.V.; M.C. wrote
493 the manuscript with the inputs from all the coauthors.

494

495 **Competing interests**

496 The authors declare that they have no conflict of interest.

497

498

499 **Acknowledgements**

500 This research was supported by the U.S. Department of Energy, Office of Science, as part of research
501 in Multi-Sector Dynamics, Earth and Environmental System Modeling Program.

502

503

504 **References**

- 505 Ashlock, D.: *Evolutionary Computation for Modeling and Optimization*, Springer-Verlag, New York.,
506 2006.
- 507 Beven, K. and Freer, J.: Equifinality, data assimilation, and uncertainty estimation in mechanistic
508 modelling of complex environmental systems using the GLUE methodology, *J. Hydrol.*, 249(1–4), 11–29,
509 doi:[http://dx.doi.org/10.1016/S0022-1694\(01\)00421-8](http://dx.doi.org/10.1016/S0022-1694(01)00421-8), 2001.
- 510 Brovkin, V., Boysen, L., Arora, V. K., Boisier, J. P., Cadule, P., Chini, L., Claussen, M., Friedlingstein,
511 P., Gayler, V., van den Hurk, B. J. J. M., Hurtt, G. C., Jones, C. D., Kato, E., de Noblet-Ducoudré, N.,
512 Pacifico, F., Pongratz, J. and Weiss, M.: Effect of Anthropogenic Land-Use and Land-Cover Changes on
513 Climate and Land Carbon Storage in CMIP5 Projections for the Twenty-First Century, *J. Clim.*, 26(18),
514 6859–6881, doi:10.1175/JCLI-D-12-00623.1, 2013.
- 515 Chong, E. K. P. and Zak, S. H.: *An introduction to optimization*, 4th Edition, John Wiley & Sons, Inc.,
516 Hoboken, NJ., 2013.
- 517 Costa, M. H. and Foley, J. A.: Combined Effects of Deforestation and Doubled Atmospheric CO₂
518 Concentrations on the Climate of Amazonia, *J. Clim.*, 13(1), 18–34, doi:10.1175/1520-
519 0442(2000)013<0018:CEODAD>2.0.CO;2, 2000.
- 520 Dickinson, R. E. and Kennedy, P.: Impacts on regional climate of Amazon deforestation, *Geophys. Res.*
521 *Lett.*, 19(19), 1947–1950, doi:10.1029/92GL01905, 1992.
- 522 Edmonds, J. and Reilly, J.: *Global Energy: Assessing the Future*, Oxford University Press, New York.,
523 1985.
- 524 Edmonds, J., Wise, M., Pitcher, H., Richels, R., Wigley, T. and Maccracken, C.: An integrated
525 assessment of climate change and the accelerated introduction of advanced energy technologies, *Mitig.*
526 *Adapt. Strateg. Glob. Chang.*, 1(4), 311–339, doi:10.1007/BF00464886, 1997.
- 527 Edmonds, J. A., Calvin, K. V., Clarke, L. E., Janetos, A. C., Kim, S. H., Wise, M. A. and McJeon, H. C.:
528 Integrated Assessment Modeling, in *Encyclopedia of Sustainability Science and Technology*, edited by R.
529 A. Meyers, pp. 5398–5428, Springer New York, New York, NY., 2012.
- 530 Elvidge, C. D., Sutton, P. C., Tuttle, B. T., Ghosh, T. and Baugh, K. E.: Global urban mapping based on
531 nighttime lights, *Glob. Mapp. Hum. Settl.*, 129–144, 2009.
- 532 FAO/IIASA/ISRIC/ISSCAS/JRC: *Harmonized World Soil Database (version 1.2)*, FAO, Rome, Italy and
533 IIASA, Laxenburg, Austria., 2012.
- 534 Findell, K. L., Berg, A., Gentile, P., Krasting, J. P., Lintner, B. R., Malyshev, S., Santanello, J. A. and
535 Shevliakova, E.: The impact of anthropogenic land use and land cover change on regional climate
536 extremes, *Nat. Commun.*, 8(1), 989, doi:10.1038/s41467-017-01038-w, 2017.
- 537 Friedl, M. A., McIver, D. K., Hodges, J. C. F., Zhang, X. Y., Muchoney, D., Strahler, A. H., Woodcock,
538 C. E., Gopal, S., Schneider, A., Cooper, A., Baccini, A., Gao, F. and Schaaf, C.: Global land cover

539 mapping from MODIS: algorithms and early results, *Remote Sens. Environ.*, 83(1), 287–302,
540 doi:[https://doi.org/10.1016/S0034-4257\(02\)00078-0](https://doi.org/10.1016/S0034-4257(02)00078-0), 2002.

541 Georgescu, M., Moustauoui, M., Mahalov, A. and Dudhia, J.: Summer-time climate impacts of projected
542 megapolitan expansion in Arizona, *Nat. Clim. Chang.*, 3, 37 [online] Available from:
543 <https://doi.org/10.1038/nclimate1656>, 2012.

544 Hansen, M. C., Defries, R. S., Townshend, J. R. G. and Sohlberg, R.: Global land cover classification at 1
545 km spatial resolution using a classification tree approach, *Int. J. Remote Sens.*, 21(6–7), 1331–1364,
546 doi:10.1080/014311600210209, 2000.

547 Hibbard, K. A. and Janetos, A. C.: The regional nature of global challenges: a need and strategy for
548 integrated regional modeling, *Clim. Change*, 118(3), 565–577, doi:10.1007/s10584-012-0674-3, 2013.

549 Hibbard, K. A., Hoffman, F. M., Huntzinger, D. and West, T. O.: Changes in land cover and terrestrial
550 biogeochemistry, in *Climate Science Special Report: Fourth National Climate Assessment, Volume I*,
551 edited by D. J. Wuebbles, D. W. Fahey, K. A. Hibbard, D. J. Dokken, B. C. Stewart, and T. K. Maycock,
552 pp. 277–302, U.S. Global Change Research Program, Washington, DC, USA., 2017.

553 Houet, T., Grémont, M., Vacqu  , L., Forget, Y., Marriotti, A., Puissant, A., Bernardie, S., Thiery, Y.,
554 Vandromme, R. and Grandjean, G.: Downscaling scenarios of future land use and land cover changes
555 using a participatory approach: an application to mountain risk assessment in the Pyrenees (France), *Reg.*
556 *Environ. Chang.*, 17(8), 2293–2307, doi:10.1007/s10113-017-1171-z, 2017.

557 Hurtt, G., Chini, L., Frolking, S., Betts, R., Feddema, J., Fischer, G., Fisk, J., Hibbard, K., Houghton, R.,
558 Janetos, A., Jones, C., Kindermann, G., Kinoshita, T., Klein Goldewijk, K., Riahi, K., Shevliakova, E.,
559 Smith, S., Stehfest, E., Thomson, A., Thornton, P., van Vuuren, D. and Wang, Y.: Harmonization of land-
560 use scenarios for the period 1500–2100: 600 years of global gridded annual land-use transitions, wood
561 harvest, and resulting secondary lands, *Clim. Change*, 109(1), 117–161, doi:10.1007/s10584-011-0153-2,
562 2011.

563 Jones, P. D., Groisman, P. Y., Coughlan, M., Plummer, N., Wang, W.-C. and Karl, T. R.: Assessment of
564 urbanization effects in time series of surface air temperature over land, *Nature*, 347(6289), 169–172,
565 doi:10.1038/347169a0, 1990.

566 Kalnay, E.: *Atmospheric modeling, data assimilation and predictability*, Cambridge University Press.,
567 2002.

568 Kim, S. H., Edmonds, J., Lurz, J., Smith, S. J. and Wise, M.: The ObJECTS Framework for Integrated
569 Assessment: Hybrid Modeling of Transportation, *Energy J.*, (Special Issue #2), 51–80, 2006.

570 Law, B. E., Hudiburg, T. W., Berner, L. T., Kent, J. J., Buotte, P. C. and Harmon, M. E.: Land use
571 strategies to mitigate climate change in carbon dense temperate forests, *Proc. Natl. Acad. Sci.*, 115(14),
572 3663 LP-3668 [online] Available from: <http://www.pnas.org/content/115/14/3663.abstract>, 2018.

573 Lawrence, D. M., Hurtt, G. C., Armeth, A., Brovkin, V., Calvin, K. V., Jones, A. D., Jones, C. D.,

574 Lawrence, P. J., de Noblet-Ducoudré, N., Pongratz, J., Seneviratne, S. I. and Shevliakova, E.: The Land
575 Use Model Intercomparison Project (LUMIP) contribution to CMIP6: rationale and experimental design,
576 *Geosci. Model Dev.*, 9(9), 2973–2998, doi:10.5194/gmd-9-2973-2016, 2016.

577 Lawrence, P. J., Feddema, J. J., Bonan, G. B., Meehl, G. A., O'Neill, B. C., Oleson, K. W., Levis, S.,
578 Lawrence, D. M., Kluzek, E., Lindsay, K. and Thornton, P. E.: Simulating the Biogeochemical and
579 Biogeophysical Impacts of Transient Land Cover Change and Wood Harvest in the Community Climate
580 System Model (CCSM4) from 1850 to 2100, *J. Clim.*, 25(9), 3071–3095, doi:10.1175/JCLI-D-11-
581 00256.1, 2012.

582 Li, X. and Zhou, Y.: A Stepwise Calibration of Global DMSP/OLS Stable Nighttime Light Data (1992–
583 2013), *Remote Sens.*, 9(6), doi:10.3390/rs9060637, 2017a.

584 Li, X. and Zhou, Y.: Urban mapping using DMSP/OLS stable night-time light: a review, *Int. J. Remote*
585 *Sens.*, 38(21), 6030–6046, doi:10.1080/01431161.2016.1274451, 2017b.

586 Liu, J., Zhang, Z., Xu, X., Kuang, W., Zhou, W., Zhang, S., Li, R., Yan, C., Yu, D., Wu, S. and Jiang, N.:
587 Spatial patterns and driving forces of land use change in China during the early 21st century, *J. Geogr.*
588 *Sci.*, 20(4), 483–494, doi:10.1007/s11442-010-0483-4, 2010.

589 Loveland, T. R., Reed, B. C., Brown, J. F., Ohlen, D. O., Zhu, Z., Yang, L. and Merchant, J. W.:
590 Development of a global land cover characteristics database and IGBP DISCover from 1 km AVHRR
591 data, *Int. J. Remote Sens.*, 21(6–7), 1303–1330, doi:10.1080/014311600210191, 2000.

592 Meiyappan, P., Dalton, M., O'Neill, B. C. and Jain, A. K.: Spatial modeling of agricultural land use
593 change at global scale, *Ecol. Modell.*, 291, 152–174, doi:https://doi.org/10.1016/j.ecolmodel.2014.07.027,
594 2014.

595 Merckx, T., Souffreau, C., Kaiser, A., Baardsen, L. F., Backeljau, T., Bonte, D., Brans, K. I., Cours, M.,
596 Dahirel, M., Debortoli, N., De Wolf, K., Engelen, J. M. T., Fontaneto, D., Gianuca, A. T., Govaert, L.,
597 Hendrickx, F., Hignati, J., Lens, L., Martens, K., Matheve, H., Matthysen, E., Piano, E., Sablon, R., Schön,
598 I., Van Doninck, K., De Meester, L. and Van Dyck, H.: Body-size shifts in aquatic and terrestrial urban
599 communities, *Nature*, 558(7708), 113–116, doi:10.1038/s41586-018-0140-0, 2018.

600 Oskins, A. J., Alex, B., James, G., Tom, H., N., H. L., Chris, W., J., W. K. and Simon, F.: Downscaling
601 land-use data to provide global 30" estimates of five land-use classes, *Ecol. Evol.*, 6(9), 3040–3055,
602 doi:10.1002/ece3.2104, 2016.

603 Le Page, Y., West, T. O., Link, R. and Patel, P.: Downscaling land use and land cover from the Global
604 Change Assessment Model for coupling with Earth system models, *Geosci. Model Dev.*, 9(9), 3055–
605 3069, doi:10.5194/gmd-9-3055-2016, 2016.

606 Piao, S., Friedlingstein, P., Ciais, P., de Noblet-Ducoudré, N., Labat, D. and Zaehle, S.: Changes in
607 climate and land use have a larger direct impact than rising CO₂ on global river
608 runoff trends, *Proc. Natl. Acad. Sci.*, 104(39), 15242 LP-15247 [online] Available from:

609 <http://www.pnas.org/content/104/39/15242.abstract>, 2007.

610 Pongratz, J., Bounoua, L., DeFries, R. S., Morton, D. C., Anderson, L. O., Mauser, W. and Klink, C. A.:
611 The Impact of Land Cover Change on Surface Energy and Water Balance in Mato Grosso, Brazil, *Earth*
612 *Interact.*, 10(19), 1–17, doi:10.1175/EI176.1, 2006.

613 Prestele, R., Armeth, A., Bondeau, A., de Noblet-Ducoudré, N., Pugh, T. A. M., Sitch, S., Stehfest, E. and
614 Verburg, P. H.: Current challenges of implementing anthropogenic land-use and land-cover change in
615 models contributing to climate change assessments, *Earth Syst. Dynam.*, 8(2), 369–386, doi:10.5194/esd-
616 8-369-2017, 2017.

617 Saltelli, A., Tarantola, S., Campolongo, F. and Ratto, M.: *Sensitivity Analysis in Practice: A Guide to*
618 *Assessing Scientific Models*, Wiley. [online] Available from:
619 <http://books.google.com/books?id=NsAVmohPNpQC>, 2004.

620 Sleeter, B. M., Liu, J., Daniel, C., Rayfield, B., Sherba, J., Hawbaker, T. J., Zhu, Z., Selmants, P. C. and
621 Loveland, T. R.: Effects of contemporary land-use and land-cover change on the carbon balance of
622 terrestrial ecosystems in the United States, *Environ. Res. Lett.*, 13(4), 45006 [online] Available from:
623 <http://stacks.iop.org/1748-9326/13/i=4/a=045006>, 2018.

624 Souty, F., Brunelle, T., Dumas, P., Dorin, B., Ciais, P., Crassous, R., Müller, C. and Bondeau, A.: The
625 Nexus Land-Use model version 1.0, an approach articulating biophysical potentials and economic
626 dynamics to model competition for land-use, *Geosci. Model Dev.*, 5(5), 1297–1322, doi:10.5194/gmd-5-
627 1297-2012, 2012.

628 Taylor, K. E., Stouffer, R. J. and Meehl, G. A.: An Overview of CMIP5 and the Experiment Design, *Bull.*
629 *Am. Meteorol. Soc.*, 93(4), 485–498, doi:10.1175/BAMS-D-11-00094.1, 2012.

630 Vernon, C. R., Le Page, Y., Chen, M., Huang, M., Calvin, K. V., Kraucunas, I. P. and Braun, C. J.:
631 Demeter—A Land Use and Land Cover Change Disaggregation Model, *J. Open Res. Softw.*, 6(1), 2018.

632 West, T. O., Le Page, Y., Huang, M., Wolf, J. and Thomson, A. M.: Downscaling global land cover
633 projections from an integrated assessment model for use in regional analyses: results and evaluation for
634 the US from 2005 to 2095, *Environ. Res. Lett.*, 9(6), 64004, 2014.

635 Ypma, T.: Historical Development of the Newton–Raphson Method, *SIAM Rev.*, 37(4), 531–551,
636 doi:10.1137/1037125, 1995.

637 Zhang, W., Villarini, G., Vecchi, G. A. and Smith, J. A.: Urbanization exacerbated the rainfall and
638 flooding caused by hurricane Harvey in Houston, *Nature*, 563(7731), 384–388, doi:10.1038/s41586-018-
639 0676-z, 2018.

640 Zhang, X., Friedl, M. A., Schaaf, C. B., Strahler, A. H., Hodges, J. C. F., Gao, F., Reed, B. C. and Huete,
641 A.: Monitoring vegetation phenology using MODIS, *Remote Sens. Environ.*, 84(3), 471–475,
642 doi:[http://dx.doi.org/10.1016/S0034-4257\(02\)00135-9](http://dx.doi.org/10.1016/S0034-4257(02)00135-9), 2003.

643 Zhou, Y., Smith, S. J., Elvidge, C. D., Zhao, K., Thomson, A. and Imhoff, M.: A cluster-based method to

644 map urban area from DMSP/OLS nightlights, *Remote Sens. Environ.*, 147, 173–185,
645 doi:<https://doi.org/10.1016/j.rse.2014.03.004>, 2014.
646